Evaluation of Integration Methods for Time-Domain Response Analysis of Vibrations in a Full-Car Model of a Rural Vehicle

Victor Provensi Mondin[1], Gustavo Comerlato Rodrigues[1], Leandro Rubén González[1], Tarik Aziz Saded Din de Souza[1], and Letícia Fleck Fadel Miguel[1]

[1]Graduate Program in Mechanical Engineering (PROMEC), Federal University of Rio Grande do Sul
425 Sarmento Leite Street, 90050-170, Rio Grande do Sul, Brazil.
victormondin@outlook.com, gustavocomerlato@gmail.com, leorubengonzalez@gmail.com,
tarik.sadeddin@hotmail.com, letffm@ufrgs.br

Abstract. Vibrations generated by road surface irregularities are intrinsically linked to the comfort level experienced by drivers and passengers in several means of transport. Consequently, the effects can range from mild discomfort to permanent trauma, depending on the vibration amplitude and exposure time. This effect is further exacerbated when traversing off-road terrain. Therefore, this study aims to determine the time-domain system responses and investigate system transmissibility in an 8-degree-of-freedom full-car vehicle model of a vehicle used in rural areas. To achieve this, a class E road surface according to ISO 8608 was generated for all four wheels using power spectral density and transformed into its corresponding time-domain representation. The system's natural frequencies and vibration modes were calculated using the vehicle's input data. Three integration methods (Newmark, Central Finite Differences, and State Space) were used to obtain the displacements and accelerations of both the vehicle body and the driver's seat, demonstrating the equivalence of the methods.

Keywords: Integration methods; full-car model; Vehicle dynamics; ISO 8608; ISO 2631-1.

1 Introduction

Technological advancements in the automotive industry have focused on reducing vehicle vibrations to improve user experience. As Harrison [1] notes, vibrations from sources like engine operation and road conditions can affect passenger comfort and vehicle durability. This has spurred the development of vibration mitigation technologies. Uneven surfaces on secondary and off-road terrains increase vibrations, impacting vehicles and potentially affecting the health of professional drivers who travel long distances. In Brazil, the NHO-09 standard [2], based on ISO 2631-1 [3], sets limits for occupational exposure to whole-body vibrations. Fossati et al. [4] used Newmark's method in a numerical analysis to show that optimized suspension systems can reduce RMS acceleration. Colpo [5] examined active control in vehicle seats under random road excitations using the state-space method, while Oliveira et al. [6] studied vertical dynamics models with different degrees of freedom using the Central Finite Differences method to understand tire-wheel behavior. These studies demonstrate various integration methods for vibration analysis. This paper aims to compare these methods and evaluate their effectiveness for this case. Despite these efforts, Zanol [7] highlights that data on workers' exposure to vibrations remains insufficient. Thus, another objective of this study is to analyze the acceleration levels experienced by drivers in specific vehicles.

2 Methodology

A routine was developed in MATLAB composed of 5 parts to evaluate the rural vehicle's dynamic response. The first part gets the inputs from the vehicle's geometry, suspension system, and the mass, stiffness, and damping matrices, that are used to calculate the dynamic matrix. The second part generates the road surface roughness profiles from power spectral density functions and converts them into time-domain signals, plotting the graphic. The third and the fourth parts calculate the numerical integration of the equations of motion using Newmark's method and Finite Differences, respectively. Finally, the fifth part also performs the numerical integration but with Space States.

2.1 Road profile modeling in the frequency domain

According to ISO 8608 [8], the road profile can be described by the Power Spectral Density (PSD) of its vertical displacement. The eq. (1) for calculating the PSD of vertical displacements is provided by Sekulic et al. [9] and can be expressed in terms of the temporal frequency f as shown below:

$$G_d(f) = v^{w-1} G_d(n_0) * \left(\frac{n}{v}\right)^{-w} \tag{1}$$

where v is the vehicle speed, $G_d(n_0)$ is the roughness coefficient, in m³, n_0 is the reference spatial frequency, in cycles/m, and w is the PSD adjustment exponent. According to the ISO 8608 [8] standard, n_0 = 0.1 cycles/m and w = 2 are used for vehicles traveling at constant speed. As stated by ISO 8608 [8], roughness coefficients are defined for eight classes of roads by their qualities. In this research, a class E road was considered to simulate the rough terrain conditions in which rural vehicles transit.

To model another road profile, it is assumed, according to ISO 8608 [8], that it is isotropic. This means that all profiles of a given road section, regardless of orientation and location, have the same properties and the coherence function resulting from this assumption is accepted. Fossati et al. [4], adopt the following dimensionless coherence function shown in eq. (2):

$$\gamma(f) = \frac{{v^2}_l}{{v^2}_l + \left(\frac{f}{v}\right)^2} \tag{2}$$

where v_l is an experimentally determined cut-off frequency in cycles/m, f is the temporal frequency in Hz, and v is the vehicle speed in m/s. The value of v_l is set at 0.2 cycles/m. Using this correlation equation, the vertical displacements of the right wheel can be determined as given by eq. (3):

$$G_{de}(f) = \gamma(f) * G_d(f) \tag{3}$$

The rear wheels are subjected to the same roughness profile as the front ones with a specific delay since they are aligned. This delay (T) is determined by the ratio between the wheelbase (l) and the vehicle's speed (v), and can be applied using a Heaviside function to the front profiles as eq. (4).

$$f_t(\mathrm{t}) = \mathrm{f}(\mathrm{t} - \mathrm{T})\mathrm{u}(\mathrm{t} - \mathrm{T}) \tag{4}$$

Proposed by Shinozuka and Jan [10], eq. (5) allows deriving a signal from the PSD in the frequency domain that represents the road profile in the time domain.

$$\vec{z}(t) = \sum_{k=1}^{N} \sqrt{2G_d^*(f_k)\Delta f_k}\ cos(2\pi f_k t + \psi_k) \tag{5}$$

where N is the number of intervals in the frequency domain, $G_d(f_k)$ is the PSD of the right front wheel, Δf_k

is the frequency resolution, and ψ_k is an independent random phase angle uniformly distributed between 0 and 2π.

2.2 Dynamic Analysis

To more accurately simulate real dynamic phenomena and analyze vibrational actions in a road vehicle, the modeling process requires a higher level of precision, particularly in the number of degrees of freedom (DoF). For this reason, an eight DoF full-car model was chosen to represent the rural vehicle (Figure 1).

This system includes a suspended body mass, four unsuspended masses at the vehicle's corners connected by suspension springs and dampers, and the driver's seat mass. The tires are modeled as sets of springs and damping elements in parallel. The eight degrees of freedom account for the vertical displacements, pitch, and roll of the suspended mass, the vertical displacements of the four unsuspended masses, and the driver's seat. All suspension and tire stiffness and damping elements are considered linear. It is also assumed that the center of gravity (CG) of the suspended mass is constant over time, with the suspension coordinate system fixed at the vehicle's CG and aligned with the principal body axes.

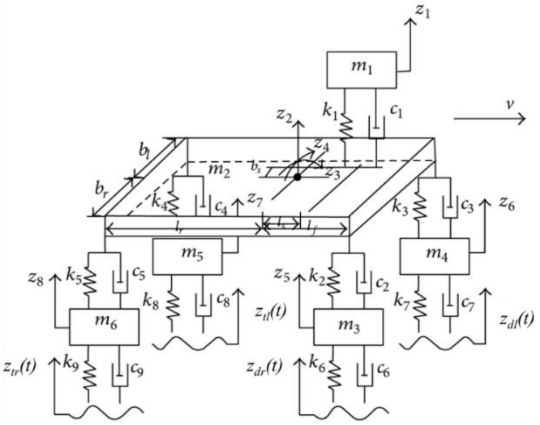

Figure 1. Dynamic model of 8 DOF for full vehicle suspension (Adapted from Fossati et al. [4]).

The mass of the driver's seat m_1, is characterized by stiffness k_1 and damping c_1. The bodywork is represented by m_2, along with its pitch and roll moments I_p and I_r. The front right and left wheels are modeled as masses m_3 and m_4, respectively, while the rear wheels are represented by masses m_5 and m_6. These unsprung masses are connected to the bodywork via springs and dampers k_2, c_2, k_3, c_3, k_4, c_4, k_5, c_5, which model the suspension system. The stiffness and damping coefficients of the tires are represented by k_6, c_6, k_7, c_7, k_8, c_8, k_9, c_9. The track excitations on the front right and left wheels are denoted by $z_{dr}(t)$ and $z_{dl}(t)$, while $z_{tr}(t)$ and $z_{tl}(t)$ represent the excitations on the right and left rear wheels. The eight DoF are represented by z_1 to z_8.

Some parameters required for the dynamic analysis were obtained directly from the vehicle manufacturer, who requested that his name not be disclosed, while others were sourced from existing literature. The vehicle's mass, including the bodywork and wheels, as well as its geometry, were provided by the vehicle manufacturer. The stiffness and damping coefficients were taken from studies by Wang et al. [11] e Xie et al. [12]. The driver's mass was estimated for an adult man. Table 1 presents the values for the parameters used in the calculations.

Table 1. Parameters with the respective values used in calculus (continue).

Variable	Description	Value	Variable	Description	Value
m_1	Mass of the driver's seat	100 kg	k_1	Seat stiffness	98935 N/m
m_2	Bodywork mass	3500 kg	k_2, k_3	Front suspension stiffness	96861 N/m
m_3, m_4, m_5, m_6	Wheels mass	44 kg	k_4, k_5	Front suspension stiffness	52310 N/m
c_1, c_6, c_7, c_8, c_9	Seat damping	615 Ns/m	k_6, k_7	Front tire stiffness	200 kN/m

Table 1. Parameters with the respective values used in calculus (conclusion).

Variable	Description	Value	Variable	Description	Value
c_2, c_3	Front suspension damping	2460 Ns/m	k_8, k_9	Rear tire stiffness	200 kN/m
c_4, c_5	Rear suspension damping	2500 Ns/m	b_l, b_r	Half of the width	1.04 m
l_f	Distance between vehicle's front and the center of gravity	1.55 m	l_r	Distance between vehicle's rear and center of gravity	1.98 m
l_s	Longitudinal distance X from seat to center of gravity	0.234 m	b_s	Transversal distance X from seat to center of gravity	0.520 m
I_r	Roll axis moment of inertia	700.7 kg.m²	I_p	Pitch axis moment of inertia	4140 kg.m²

Based on the physical model shown in Figure 1, the equations of motion for the previously identified eight degrees of freedom can be described. To simplify computational calculations, the system will be organized into matrix form, as outlined in the eq. (6):

$$\boldsymbol{M}\vec{\ddot{z}}(t) + \boldsymbol{C}\vec{\dot{z}}(t) + \boldsymbol{K}\vec{z}(t) = \vec{F}(t) \tag{6}$$

where $\boldsymbol{M}$, $\boldsymbol{C}$ and $\boldsymbol{K}$ are the matrices of mass, damping, and stiffness, respectively, $\vec{\ddot{z}}(t)$, $\vec{\dot{z}}(t)$ *e* $\vec{z}(t)$ are the vectors of acceleration, velocity, and displacement, respectively, and $\vec{F}(t)$ is the vector of external forces applied to the system.

2.3 Integration Method - Central Finite Differences (CFD)

The finite difference method, according to Rao [13], uses approximations for derivatives, replacing the differential equation of motion and boundary conditions with finite difference equations. There are three types of formulations: forward, backward, and central differences, with the latter being the most accurate. In this method, the domain is replaced by mesh points, where solution values are computed. The central difference formulas for velocity and acceleration are:

$$\dot{z}_i = \frac{z_{i+1} - z_{i-1}}{2\Delta t}, \quad \ddot{z}_i = \frac{z_{i+1} - 2z_i + z_{i-1}}{(\Delta t)^2} \tag{7}$$

For systems with multiple degrees of freedom and viscous damping, the equation of motion will according to eq. (6). Rao [13] shows that, by isolating the displacement terms, the equation of motion at time t_i can be written as:

$$\left(\frac{1}{\Delta t^2}\boldsymbol{M} + \frac{1}{2\Delta t}\boldsymbol{C}\right) z(t_{i+1}) = \boldsymbol{F}(t_i) - \left(\boldsymbol{K} - \frac{2}{\Delta t^2}\boldsymbol{M}\right) x(t_i) - \left(\frac{1}{\Delta t^2}\boldsymbol{M} - \frac{1}{2\Delta t}\boldsymbol{C}\right) x(t_{i-1}) \tag{8}$$

The values of $z(t_{i+1})$ can be determined, allowing for the calculation of velocity and acceleration.

2.4 Integration Method – Newmark

Newmark is a numerical integration method used to solve differential equations, such as dynamic equilibrium equations. The method is suitable for nonlinear structural dynamics and is expressed as:

$$z_{i+1} = z_i + \Delta t\dot{z}_i + \frac{(\Delta t)^2}{2}[(1-2\beta)\ddot{z}_i + 2\beta\ddot{z}_{i+1}] \tag{9}$$

where $z_i, \dot{z}_i$ and $\ddot{z}_i$ are the displacement, velocity, and acceleration at time t_i, Δt is the time step between successive time steps, and β and γ are parameters of the Newmark method. For this paper, it was used $\beta = 0.25$ and $\gamma = 0.5$, following Bathe [14] to guarantee the stability of the method, and Δt was set in 0,08825s by considering the dimension between axles and the vehicle speed. In this work, we implemented this method following its description as in standard engineering textbooks such as Rao (2011).

2.5 Integration method – Space-State

The state-space method is a mathematical framework used to model and analyze dynamic systems, especially those with multiple inputs and outputs. The state-space model is expressed in two primary equations:

$$\dot{q} = \boldsymbol{A}q + \boldsymbol{B}u, \qquad y = \boldsymbol{C}q + \boldsymbol{D}u \tag{10}$$

Where q is the state vector, representing the internal variables or states of the system that describe its current condition, u is the input vector, consisting of external forces or control inputs applied to the system and y is the output vector, representing the measured or controlled variables of the system. It should be noted that the matrices $\boldsymbol{A}$, $\boldsymbol{B}$, $\boldsymbol{C}$, and $\boldsymbol{D}$ for a given system are not unique, leading to multiple possible representations for the same system. Additional information about the method is explained by Aplevich [15].

3 Results

3.1 Rural vehicle simulation

Using all the data on masses, damping coefficients, and stiffness, the dynamic matrix was calculated. From this matrix, the system's eigenvalues and eigenvectors were obtained, corresponding to the natural frequencies of vibration and the modes of vibration, respectively. Tables 2 present these data.

Table 2. Natural frequencies, in Hz, and vibration modes of the rural vehicle.

	f_1	f_2	f_3	f_4	f_5	f_6	f_7	f_8
	1.2152	1.9389	2.7872	5.2157	12.0804	12.0860	13.1248	13.1757
DoF	$\overrightarrow{C_1}$	$\overrightarrow{C_2}$	$\overrightarrow{C_3}$	$\overrightarrow{C_4}$	$\overrightarrow{C_5}$	$\overrightarrow{C_6}$	$\overrightarrow{C_7}$	$\overrightarrow{C_8}$
z_1	0.6793	-0.2696	0.5222	-0.9915	0.0005	-0.0020	-0.0013	0.0029
z_2	0.6456	-0.565	-0.0188	0.0299	-0.0038	0.0001	0.0058	-0.0001
z_3	0.0512	0.7004	0.0065	-0.0066	-0.0062	0.0001	-0.0076	0.0001
z_4	-0.109	0.0167	-0.7319	-0.1025	-0.0002	-0.0185	0.0001	0.0329
z_5	0.1835	-0.3636	-0.2699	-0.0259	0.0118	-0.0431	-0.7115	-0.7013
z_6	0.1909	-0.3752	0.2505	0.0568	0.0126	0.0432	-0.7024	0.7013
z_7	0.1588	0.2794	0.1654	0.0315	0.6987	-0.7139	0.0104	0.0363
z_8	0.1541	0.2868	-0.1680	-0.229	0.7152	0.6974	0.0102	-0.0363

The characteristics of each vibration mode can be inferred from the data presented. The first two vibration modes, with natural frequencies of 1.2152 Hz and 1.9389 Hz, primarily excite the driver's seat. The second mode also significantly affects the vertical displacement of the car body. The third and fourth modes, with natural frequencies of 2.7872 Hz and 5.2157 Hz, induce excitations in the car body's pitch and roll degrees of freedom. These first four modes are associated with lower frequencies and correspond to the suspended masses of the vehicle. In contrast, the following modes relate to the unsprung masses (i.e., the vehicle's wheels) and have higher natural frequencies. The fifth and sixth modes, with frequencies of 12.0804 Hz and 12.0806 Hz, respectively, excite the front axle wheels, while the seventh and eighth modes, with frequencies of 13.1248 Hz and 13.1757 Hz, predominantly excite the rear axle wheels. Chaffin et al. [16] note that frequencies in the range of 0 to 2 Hz can cause discomfort in humans due to interference with the vestibular system. This suggests that the first vibration modes of the seat could potentially lead to discomfort. Therefore, it is essential to compare the vibration exposure levels to which the driver is subjected with the criteria set by NHO-09 [2].

Then, it was analyzed the displacement and acceleration responses experienced by both the bodywork and the driver's seat, using the three methods, as can be seen on the Figure 2. The results demonstrate that all three integration methods yield identical displacement (Figure 2 (a)) and acceleration (Figure 2 (b)) responses. Minor variations between the methods might exist, but they are not visually significant, demonstrating the robustness of each method. Also, the synchronization between the seat and bodywork displacement responses suggests a coherent model where the seat closely follows the bodywork's vertical movements.

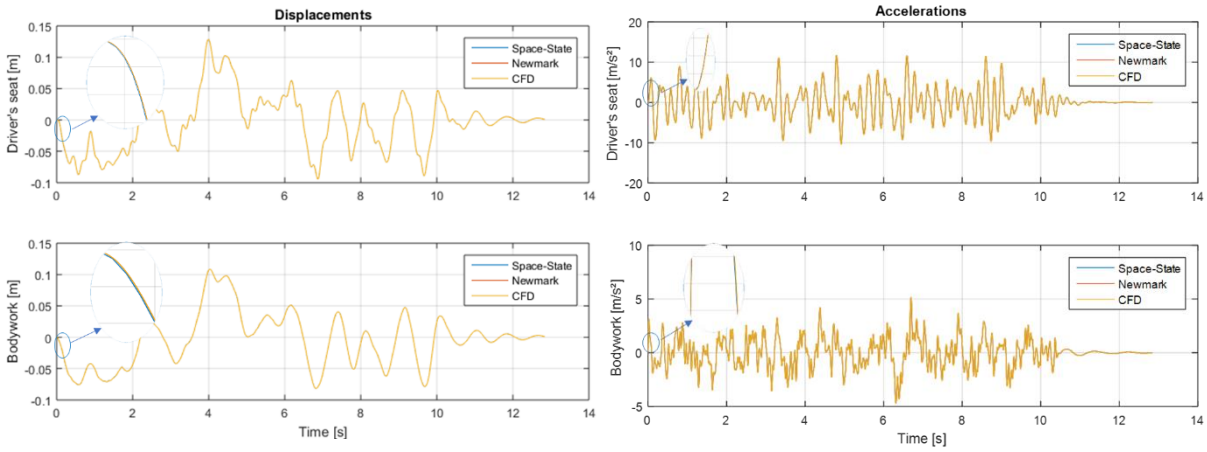

Figure 2. (a) Vertical displacement at the driver's seat and bodywork, (b) Vertical acceleration at the driver's seat and bodywork, comparing the methods.

3.2 Transmissibility

A graphical analysis of the vehicle structure was conducted to examine the frequency response of the displacements and accelerations experienced by the driver. This analysis utilized transfer functions derived from the state-space formulation, with inputs being the displacements applied to the right and left wheels. The study considered both individual tire displacements and joint displacements of tires on the same track. Figure 3 presents the transmissibility graphs for the magnitude of vertical displacement and acceleration at the driver's seat for the vehicle moving at 10 m/s.

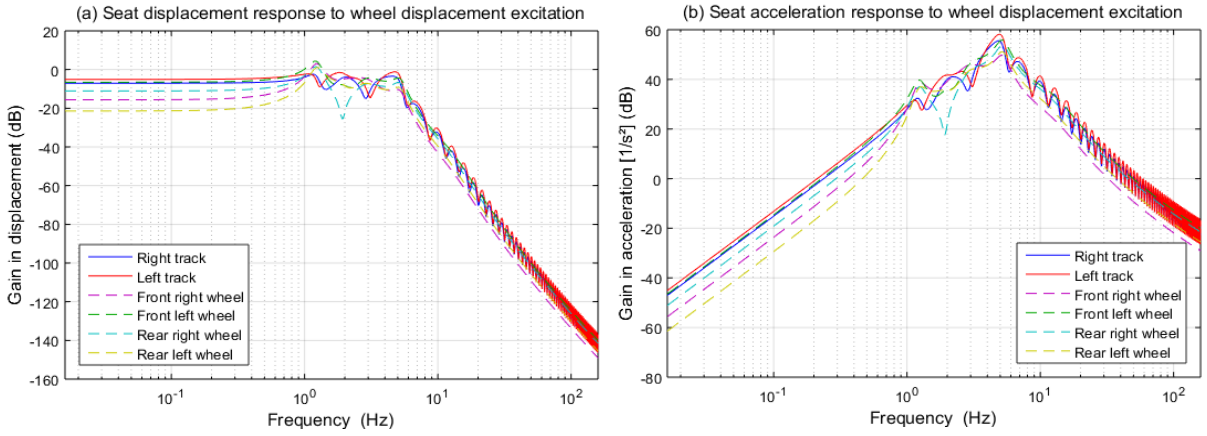

Figure 3. Magnitude response (a) on seat displacement, and (b) on seat vertical acceleration.

In Figure 3(a), a peak in magnitude is observed around 1.22 Hz in the displacement graph for individual wheel inputs, corresponding to the system's first natural frequency. For coupled inputs between two wheels on the same track, the peak is spread over a wider frequency range due to joint excitation. Figure 3(b) shows that both individual tire excitations and joint track excitations reach a maximum around 5.17 Hz, with an acceleration gain of approximately 60 decibels (or 1000 times). Additionally, the graphs indicate that coupled inputs on the same track (solid lines) display "lobes" in magnitude. This phenomenon is explained by the time delay between the movement of the front and rear tires on the same track due to vehicle speed. This delay modifies the system's frequency response by affecting the phase delay between two independent excitations for the tires on the same track. For example, if the time delay results in a 360° phase shift, both wheels would rise and fall simultaneously on the same track, which could either amplify or diminish the excitation of different system modes.

3.3 Evaluation of whole-body vibration according to NHO-09

Taking a step beyond the initially proposed scope, it was decided to evaluate the whole-body vibration exposure of the driver (first degree of freedom) according to NHO-09 [2]. This standard, in turn, is based on ISO 2631-1 [3], offering similar methods but with clearly defined values for exposure.

As presented in Section 5, *aren* is the normalized resultant acceleration of exposure and is one of the basics parameters for evaluation. Four exposure periods, each approximately one hour long, were considered during the workday. Only one component of exposure, specifically in the z-axis, was considered, in accordance with the DoF described in Section 2.2 related to driver's seat. Using the equation presented in the section, *aren* of 1.3 was obtained for the simulated profile. The daily occupational exposure limit for whole-body vibration adopted in the standard corresponds to an *aren* of 1.1 m/s². Therefore, the value found exceeds the permissible limit.

4 Conclusions

The present paper studied the dynamic analysis of a rural vehicle traveling on off-road terrain. It was demonstrated that all three integration methods used – Newmark, Central Finite Differences, and Space-States – present very similar results. Therefore, simplified methods, such as the Newmark method or the Central Finite Differences method, are suitable for integration in similar cases. For the vehicle and profile analyzed, it was concluded that the driver is exposed to a larger acceleration that is permitted by the standard, which happens often with drivers in rural areas submitted to vibrations for longer periods. Due to the lack of sufficient data for a statistical analysis, further studies in this area are necessary for more accurate conclusions regarding the epidemiological effect on drivers.

Acknowledgements. The authors would like to thank the Brazilian agencies CNPq, CAPES, and Propesq for the financial support for the publication of this paper.

Authorship statement. The authors hereby confirm that they are the sole liable persons responsible for the authorship of this work, and that all material that has been herein included as part of the present paper is either the property (and authorship) of the authors, or has the permission of the owners to be included here.

References

[1] M. Harrison. Vehicle Refinement: controlling noise and vibration in road vehicles. Warrendale: SAE International, 2004.
[2] NHO-09. Avaliação da exposição ocupacional a vibrações de corpo interno. Brazilian standard, 2013
[3] ISO 2631:1997. Mechanical Vibration and Shock– Evaluation of human exposure to whole-body vibration. Standard, International Organization for Standardization, Geneva, CH, 1995
[4] G. G. Fossati, L. F. F. Miguel, and W. J. P. Casas. Multi-objective optimization of the suspension system parameters of a full vehicle model. Optimization and Engineering, vol. 20, n. 1, pp. 151–177, 2018.
[5] L. R. Colpo, Performance of active control in a vehicle seat under random road excitations. Int. J. Dynam. Control, 2024.
[6] P. H. D. D. de Oliveira, A. M. Calhabeu, V. M. L. Lopes. Comparison and Detailing of Vertical Dynamic Models and Their Application Contexts. AEA – Brazilian Society of Automotive Engineering - SIMEA 2023
[7] E. J. Zanol, Avaliação dos níveis de vibração de corpo inteiro sofridos por motoristas de ônibus urbanos em diferentes tipos de pistas mathesis, Universidade Federal do Rio Grande do Sul, Porto Alegre, 2020.
[8] ISO 8608:2016. Mechanical Vibration–Road Surface Profiles– Reporting of Measured Data. Standard, International Organization for Standardization, Geneva, CH, 2016.
[9] D. Sekulić, V. Dedović, S. Rusov, S. Ŝalinić, and A. Obradović. Analysis of vibration effects on comfort of intercity bus users by oscillatory model with ten degrees of freedom. Applied Mathematical Modelling, 37(18-19), pp. 8629–8644, 2013.
[10] M. Shinozuka and C. M. Jan, Digital simulation of random processes and its applications, *Journal of Sound and Vibration*, vol. 25, no. 1. Elsevier BV, pp. 111–128, 1972.
[11] L. Wang, N. G. Xie, C. Z. Song, J. H. Bao, Y. W. Cen, Multi-objective bionics design method of passive suspension parameters based on hybrid behavior game, Structural and Multidisciplinary Optimization, v. 42, n. 3, p. 371 – 386, 2010
[12] N. G. Xie, R. Meng, Y. Ye, L. Wang, Y. W. Cen, Multiobjective design method based on evolution game and its application for suspension, Structural and Multidisciplinary Optimization, v. 47, n. 2, p. 207 – 220, 2013.
[13] S. S. Rao, Mechanical vibrations (5th ed). Prentice Hall, 2011
[14] K. L. Bathe, Finite Element Procedures, 2nd edition, Watertown, MA, 2014
[15] J. D. Aplevich, The essentials of linear state-space systems. Nashville, TN. John Wiley & Sons, 1999.
[16] D. B. Chaffin, G. B. J. Andersson, and B. J. Martin. Occupational Biomechanics. Wiley-Interscience, 4edition, 1999.